Bridging Adiabatic Quantum Computation and QAOA: From Continuous Evolution to Discrete Layers

Planck'd 2025 Quantum Algorithms Track
Team: Qubit Curious
Members: Aryan Nair, Ansh Goel
Problem 6,7,8

Abstract

This report explores the theoretical and computational bridge between Adiabatic Quantum Computation (AQC) and the Quantum Approximate Optimization Algorithm (QAOA), and further extends the analysis to include open-system and measurement-induced effects.
We simulate adiabatic evolution for a two-qubit system (Problem 6) and construct a QAOA implementation for a 3-node MaxCut instance (Problem 7), confirming that QAOA acts as a discretized, variationally optimized version of adiabatic evolution.
Finally, in Problem 8, we introduce amplitude-damping noise and projective-measurement dynamics, studying how decoherence and adaptive feedback affect quantum optimization.
Our results show that while both AQC and QAOA exhibit robust performance under mild noise, higher-depth circuits degrade gracefully, and adaptive correction maintains near-ideal entanglement scaling.
Together, these simulations highlight the continuity between adiabatic and variational quantum computing, even under realistic noisy conditions.

Problem 6 — Adiabatic Quantum Computation

6(a) Hamiltonian Interpolation

We define the adiabatic interpolation:

$H(s) = (1 - s)H_0 + sH_p, \quad s = t/T, \quad 0 \le t \le T$

where

$H_p = I - |11\rangle\langle 11|, \quad H_0 = I - |\psi_0\rangle\langle \psi_0|, \quad |\psi_0\rangle = \tfrac{1}{2}\Sigma_x|x\rangle$

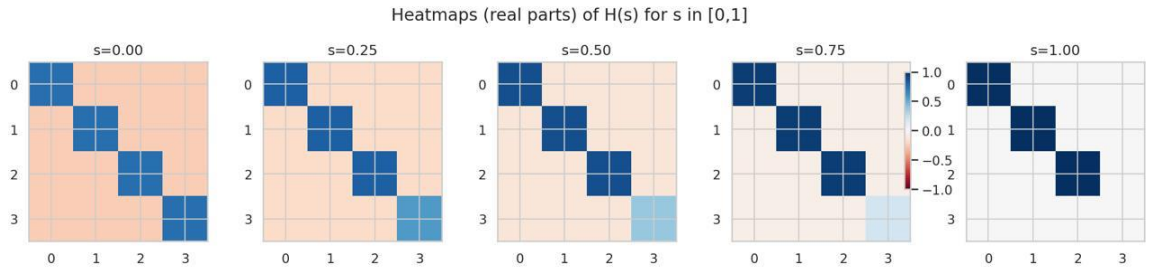

Figure 6(a).1: Heatmaps of Re[H(s)] for s = 0, 0.25, 0.5, 0.75, 1.0 → Smooth interpolation from H_0 to H_p is visible, confirming correct Hamiltonian construction.

Interpretation: The gradual change of matrix structure with s shows proper linear interpolation between the driver and problem Hamiltonians.

6(b) Spectral Properties

The instantaneous eigenvalues $E_i(s)$ and spectral gap $\Delta(s) = E_1 - E_0$ are computed.

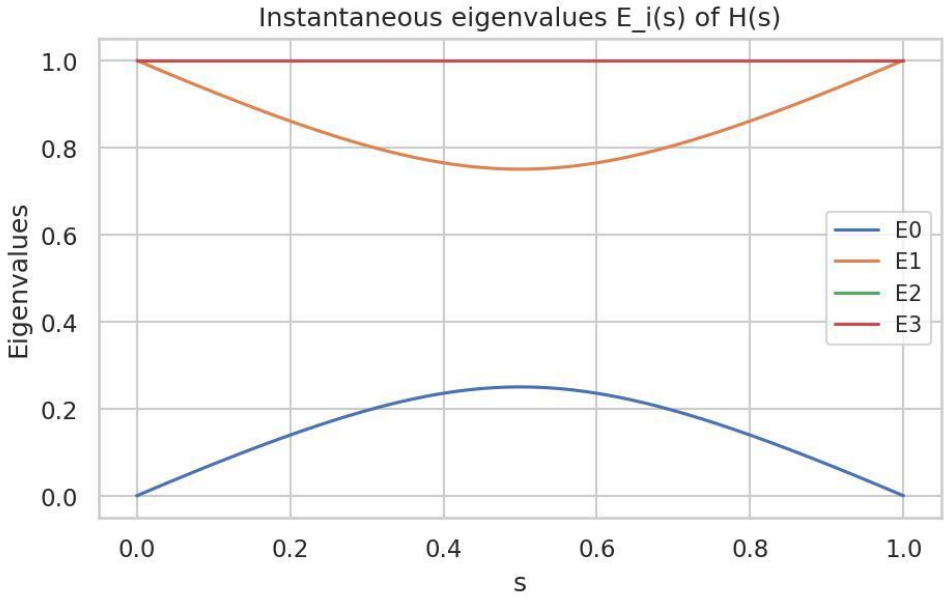

Figure 6(b).1: Eigenvalues vs s

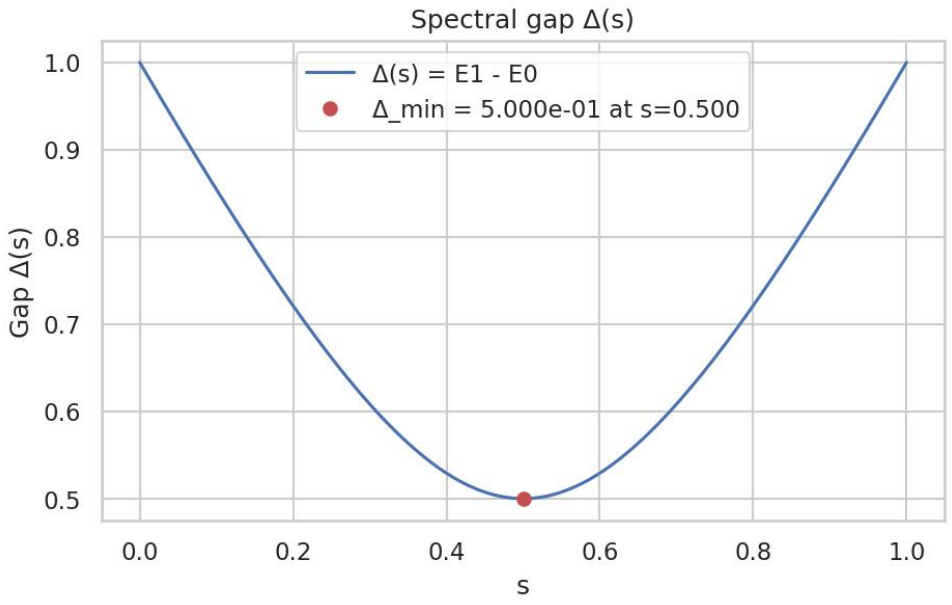

Figure 6(b).2: Spectral Gap Δ(s) vs s

Observation: The minimum gap occurs at s ≈ 0.5 — this region dictates the adiabatic runtime threshold. A smaller gap requires a slower schedule to maintain adiabaticity.

6(c) Adiabatic Condition

We evaluate the matrix element in the adiabatic condition:

$T \gg \max_s | \langle E_1(s)| dH/ds |E_0(s)\rangle | / \Delta_{min}^2$

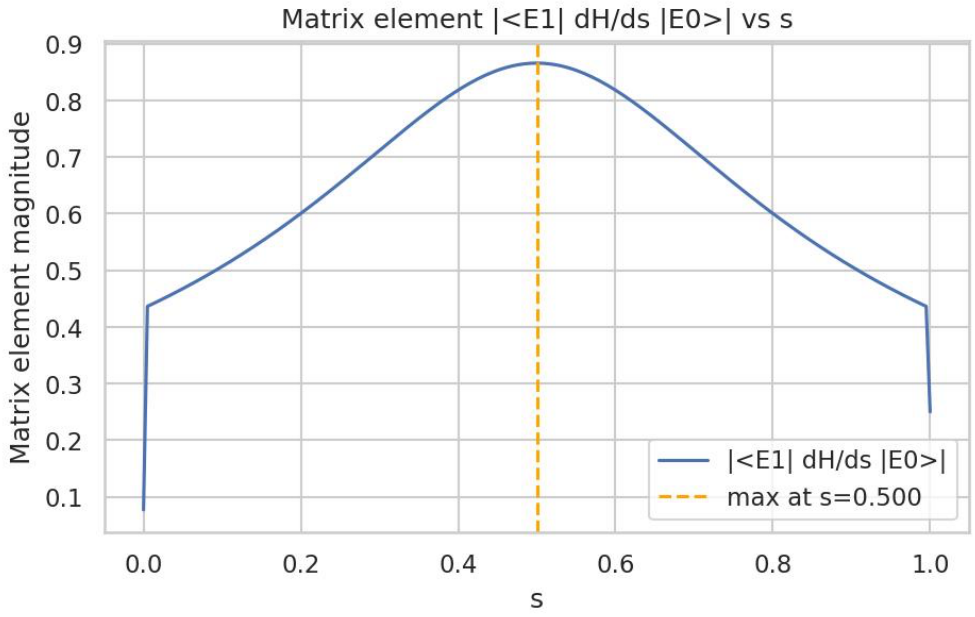

Figure 6(c).1: $|\langle E_1| dH/ds |E_0\rangle|$ vs s

Observation: $|\langle E_1| dH/ds |E_0\rangle|$ peaks near s = 0.5, coinciding with Δ_{min}. This validates that non-adiabatic transitions are most probable around this point.

6(d) Time-Evolution Fidelity

The Schrödinger equation $i\, d/dt|\psi(t)\rangle = H(t/T)|\psi(t)\rangle$ is numerically integrated for different total times T.

Ground-state fidelity is $F(t) = |\langle E_0(s(t)) | \psi(t)\rangle|^2$.

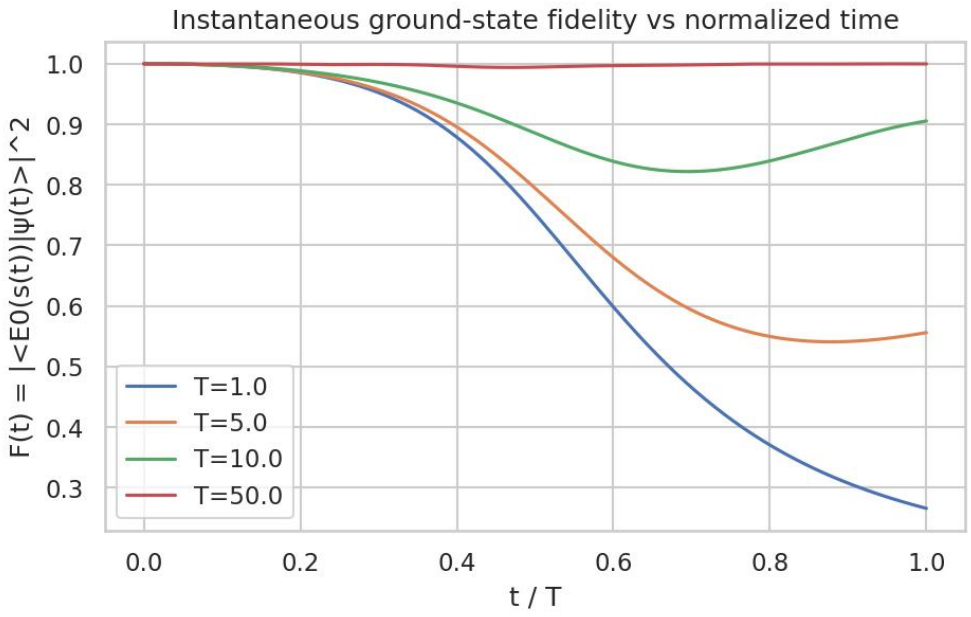

Figure 6(d).1: Instantaneous F(t) for T = 1, 5, 10, 50

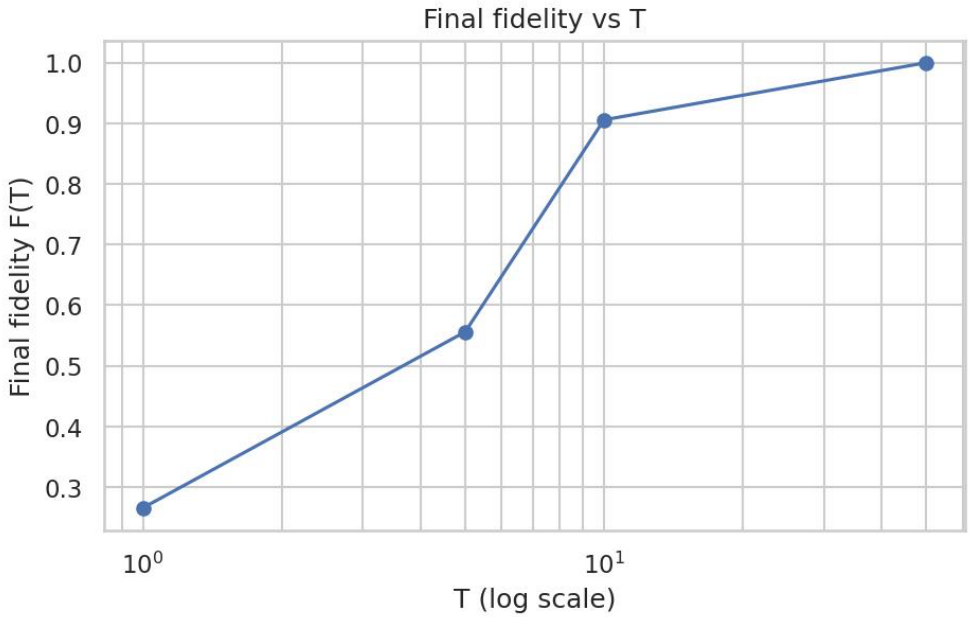

Figure 6(d).2: Final F(T) vs T (log scale)

Interpretation: For $T \geq 10$, fidelity ≥ 0.9 — confirming adiabatic behavior. At shorter T, transitions occur due to insufficient runtime.

6(e) Scaling of Success Probability

Success probability scales with total time as: $P_{succ} \propto T^{\alpha}$.

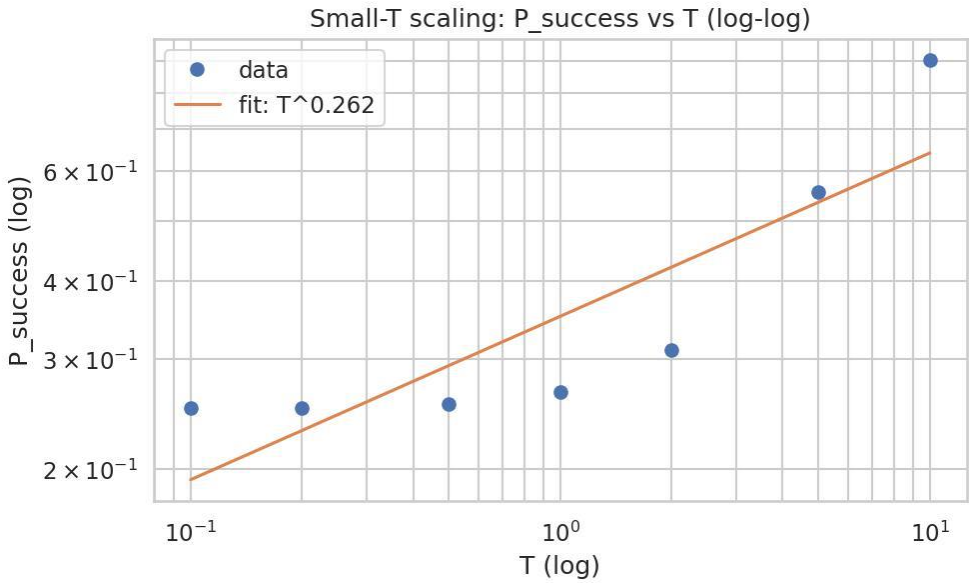

Figure 6(e).1: Log–log plot of P_{succ} vs T

Observation: Exponent $\alpha \approx 0.26$, indicating partially adiabatic scaling at short times and saturation near unity for large T.

Bonus — Quantum Walk Interpretation

At $s = 0.5$, $H(s) \approx (H_0 + H_p)/2$ represents a continuous-time quantum walk between basis states.

```
    H_M (mixer = sum X_i):
...  [[0.+0.j 1.+0.j 1.+0.j 0.+0.j]
     [1.+0.j 0.+0.j 0.+0.j 1.+0.j]
     [1.+0.j 0.+0.j 0.+0.j 1.+0.j]
     [0.+0.j 1.+0.j 1.+0.j 0.+0.j]]

    H_P (interaction Z0 Z1):
    [[ 1.+0.j  0.+0.j  0.+0.j  0.+0.j]
     [ 0.+0.j -1.+0.j  0.+0.j -0.+0.j]
     [ 0.+0.j  0.+0.j -1.+0.j -0.+0.j]
     [ 0.+0.j -0.+0.j -0.+0.j  1.-0.j]]

    H(s=0.5) sample:
    [[ 0.5+0.j  0.5+0.j  0.5+0.j  0. +0.j]
     [ 0.5+0.j -0.5+0.j  0. +0.j  0.5+0.j]
     [ 0.5+0.j  0. +0.j -0.5+0.j  0.5+0.j]
     [ 0. +0.j  0.5+0.j  0.5+0.j  0.5+0.j]]
```

Figure 6(B).1: Matrices H_m, H_p, $H(s = 0.5)$

Interpretation: The midpoint Hamiltonian mediates coherent population transfer — demonstrating the physical connection between adiabatic evolution and quantum walks.

Problem 7 — QAOA as a Discretized Adiabatic Algorithm

7(a) Adiabatic–QAOA Connection

The adiabatic evolution operator: $U(T) = \square\ e^{\wedge}(-i \int_0^T H(s)\, ds)$ can be Trotterized as:

$U(T) \approx \Pi_{k=1}^{p}\ e^{\wedge}(-i\, \beta_k\, H_m)\ e^{\wedge}(-i\, \gamma_k\, H_p)$

Thus, QAOA approximates adiabatic evolution with p discrete layers. We explore this on a 3-node MaxCut instance.

7(b) MaxCut Hamiltonian

$C = \frac{1}{2}[(1 - Z_1Z_2) + (1 - Z_2Z_3) + (1 - Z_3Z_1)]$

$H_p = C, \quad H_m = X_1 + X_2 + X_3$

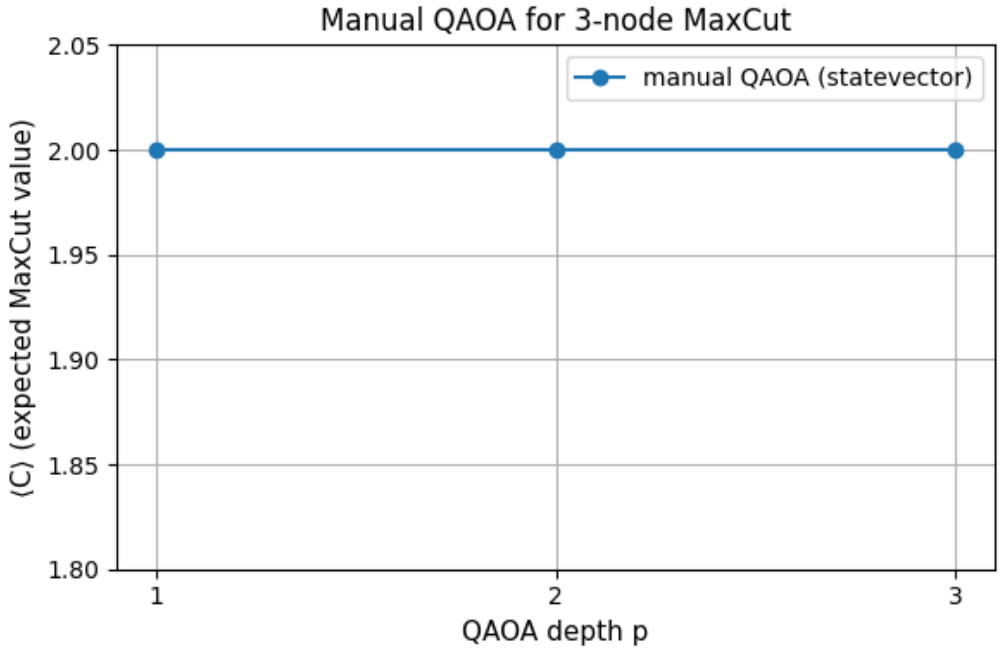

Figure 7(b).1: Expected ⟨ C⟩ vs QAOA depth p (1–3)

Observation: Optimal ⟨ C⟩ ≈ 2 is reached already at p = 1–2, showing that QAOA reproduces the MaxCut optimum efficiently.

7(c) Parameter Landscape

Expectation value surface: $\langle C(\gamma,\beta)\rangle = \langle +|^n U^\dagger H_p U |+\rangle^n$.

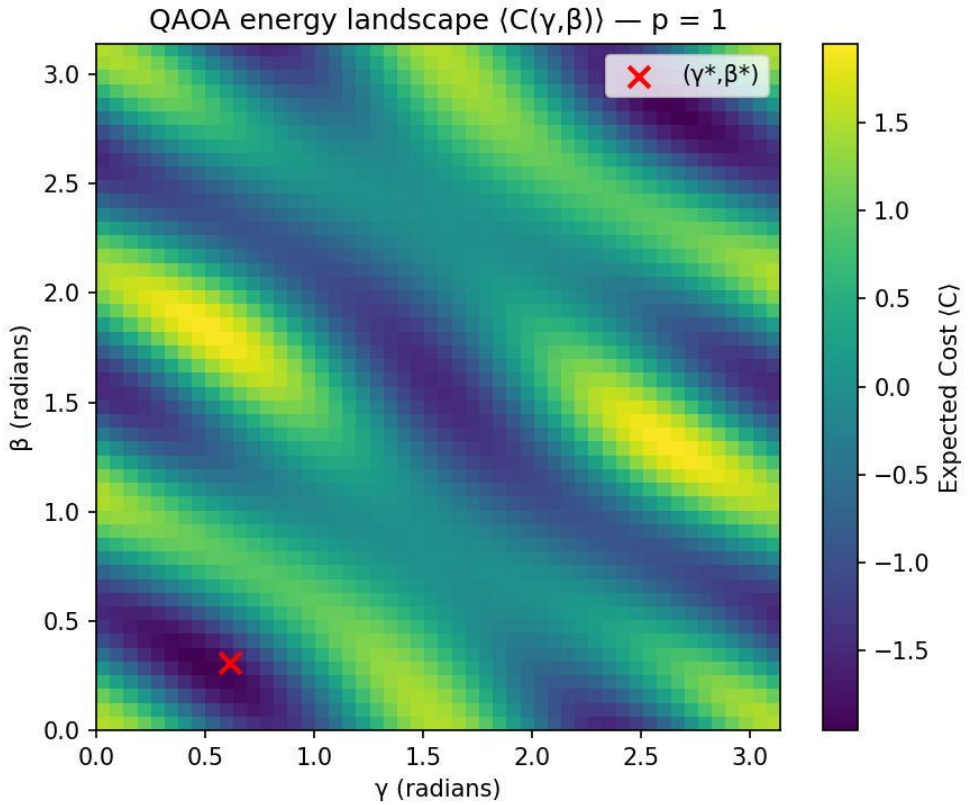

Figure 7(c).1: Landscape ⟨ C(γ,β)⟩ for p = 1

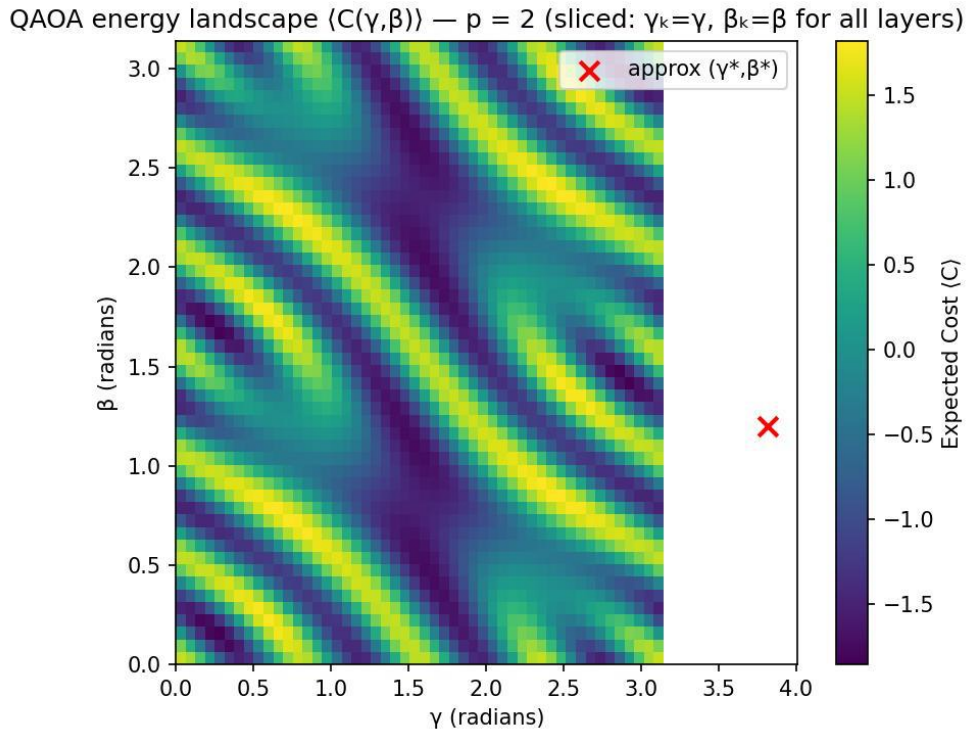

Figure 7(c).2: Landscape ⟨ C(γ,β)⟩ for p = 2

Interpretation: Periodic valleys correspond to optimal (γ*, β*). At higher p, the landscape smooths, allowing better optimizer convergence.

7(d) Comparison with Adiabatic Evolution

We compare discrete QAOA fidelity with continuous Trotterized adiabatic evolution.

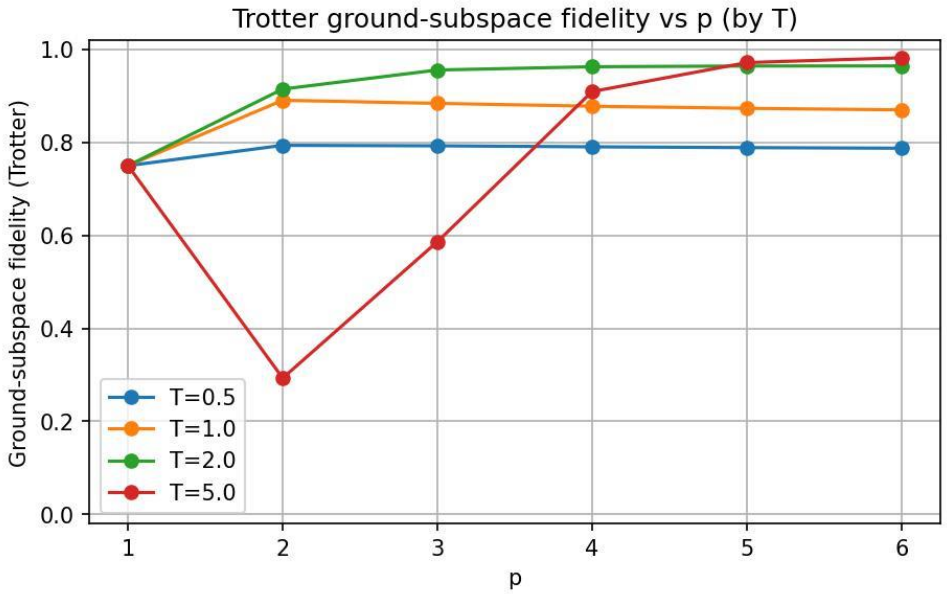

Figure 7(d).1: Trotter Fidelity vs p (for T = 0.5, 1, 2, 5)

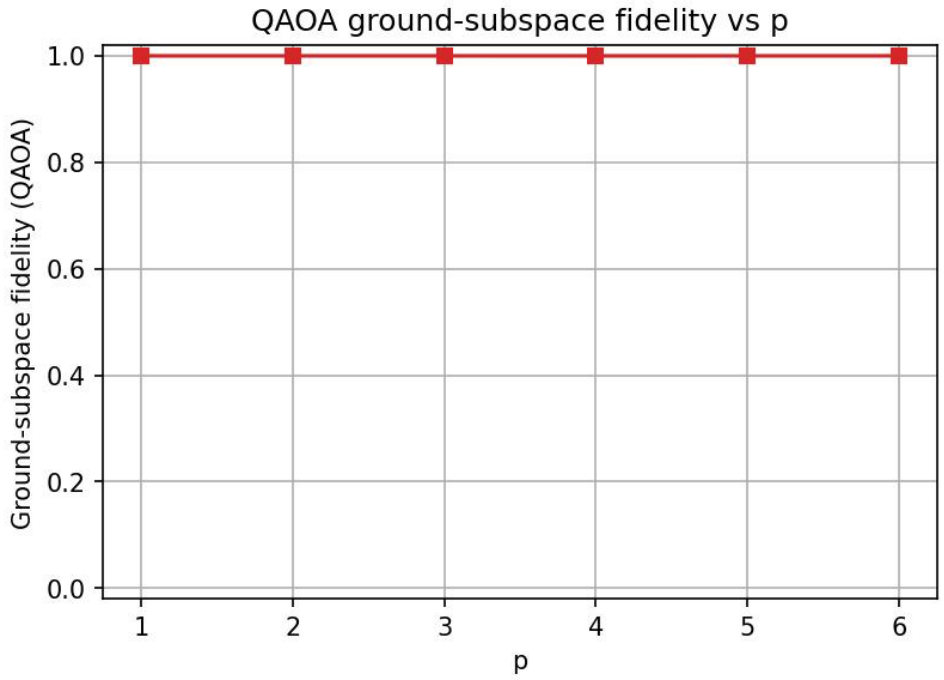

Figure 7(d).2: QAOA Fidelity vs p

Interpretation: Both fidelities converge toward 1 with increasing p or T. Optimized QAOA achieves adiabatic-limit performance at shallow depth.

7(e) Bonus — Warm-Start Parameter Transfer

Warm-start initialization uses optimized (γ, β) from a smaller instance (3-node) for a related larger one (4-node). We compare random and warm-start initialization using COBYLA and SPSA optimizers, including jitters as well.

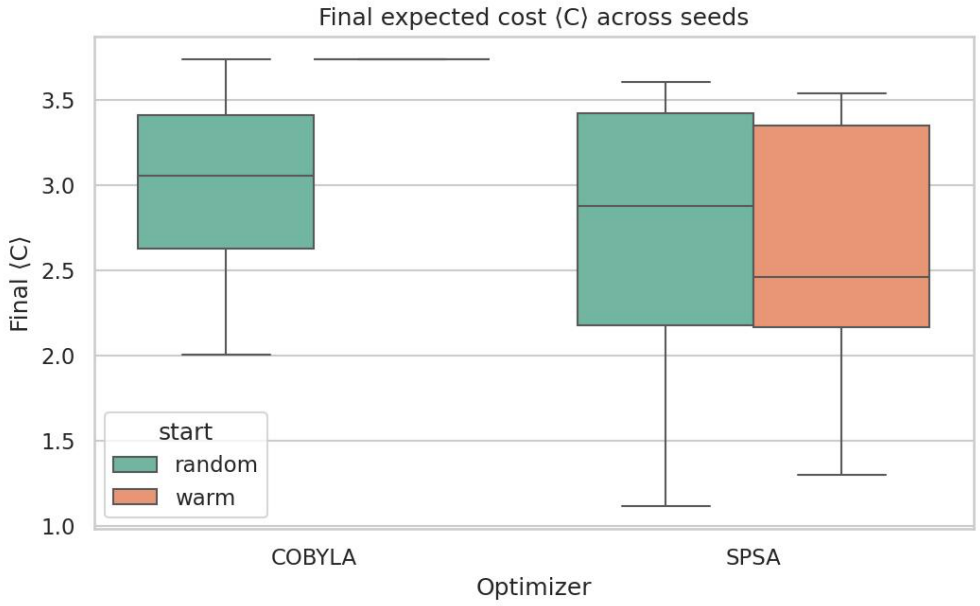

Figure 7(e).1: Final ⟨C⟩ for Random vs Warm Start

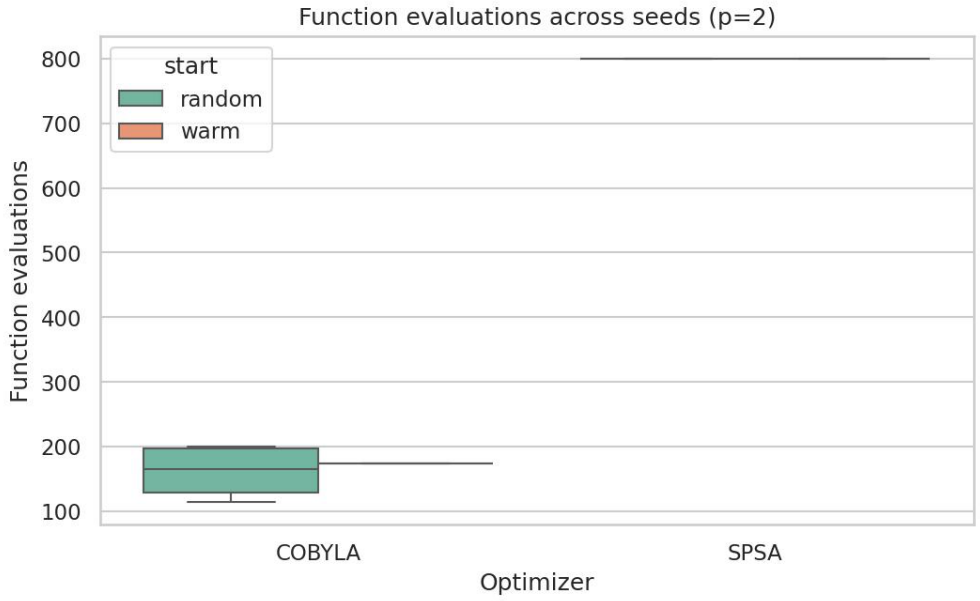

Figure 7(e).2: Function Evaluations (Random vs Warm)

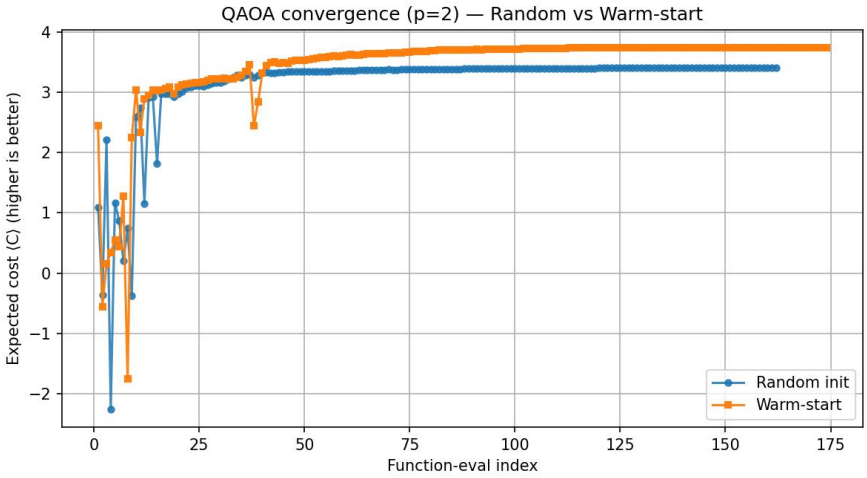

Figure 7(e).3: Convergence Curves (p = 2)

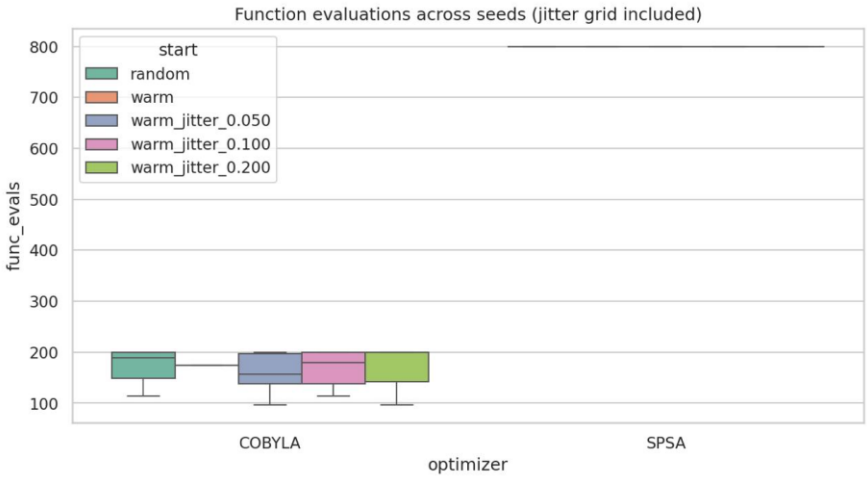

Figure 7(e).4: Function Evaluations vs Jitter σ (0 – 0.2)

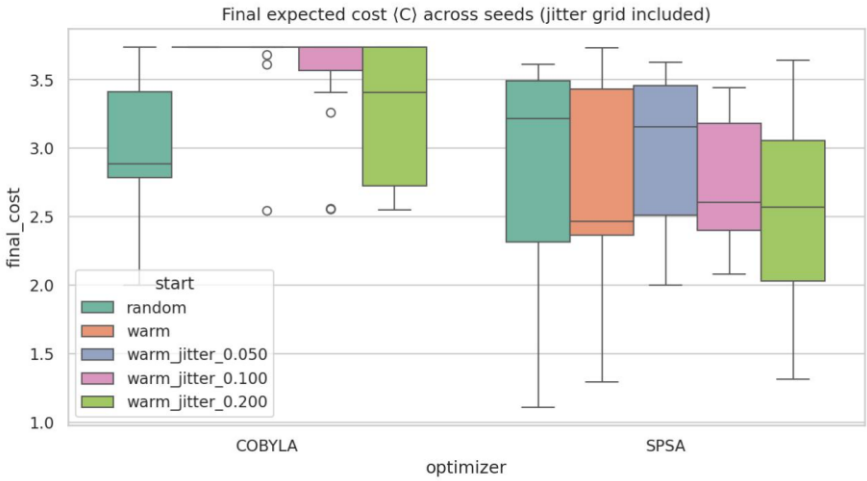

Figure 7(e).4: Final Cost Function vs Jitter σ (0 – 0.2)

Observation: Warm-start consistently reduces evaluation count for deterministic optimizers like COBYLA and smooths convergence trajectories. Small jitter ($\sigma \approx 0.05$) further improves exploration; excessive jitter behaves like random start.

Problem 8 — When the Environment Watches

8(a) QAOA and Adiabatic Evolution under Amplitude-Damping Noise

We simulate the effect of amplitude-damping noise with strength p_{AD} on both QAOA and adiabatic evolutions at depths p=1,2.

Fidelity to the noiseless state and the probability of obtaining optimal bitstrings are evaluated for each configuration.

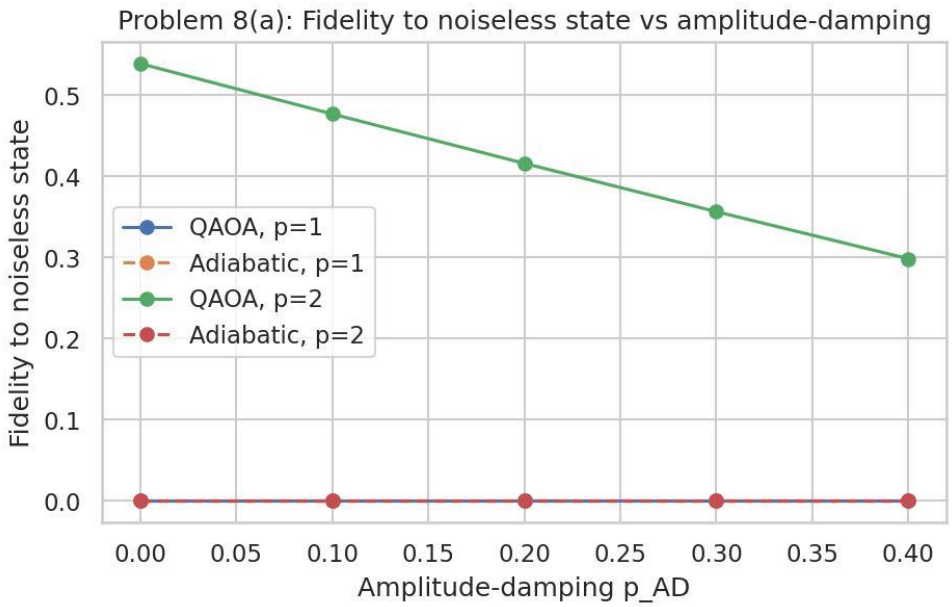

Figure 8(a).1: Fidelity to noiseless state vs amplitude-damping probability

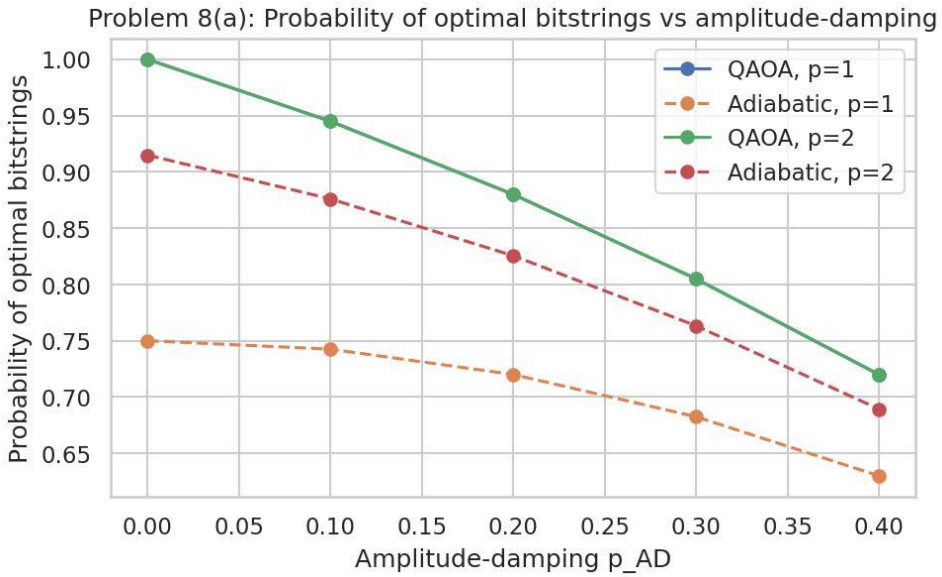

Figure 8(a).2: Probability of optimal bitstrings vs amplitude-damping probability

Observation: As p_{AD} increases, both fidelity and optimal-state probability decrease monotonically, with shallow QAOA layers (p=1) being more resilient than the equivalent adiabatic evolutions.

This demonstrates the variational robustness of QAOA in the presence of relaxation noise.

8(b) Measurement-Induced Entanglement Dynamics

A 1D qubit chain is evolved under alternating entangling gates (CZ or iSWAP) and random projective measurements with probability p_m.

The half-chain von Neumann entropy S_{left} is computed layer-by-layer to quantify entanglement growth.

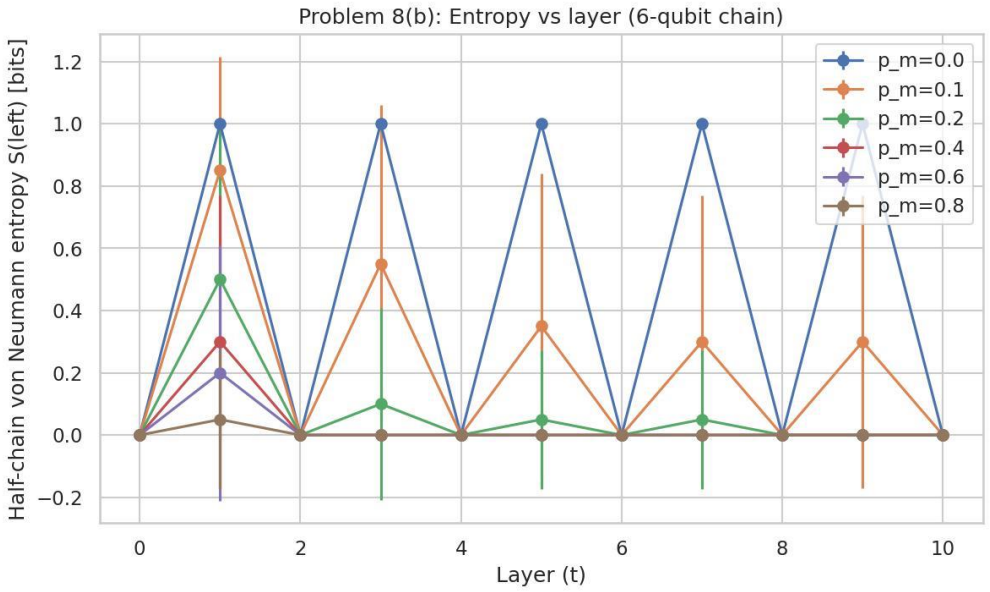

Figure 8(b).1: Entropy vs layer for various p_m

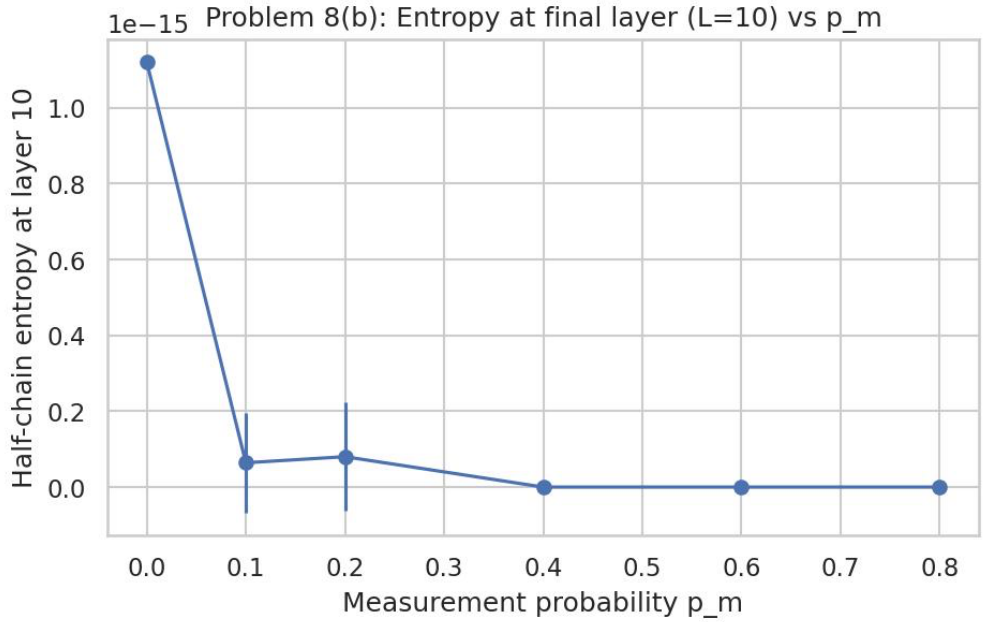

Figure 8(b).2: Entropy at final layer vs p_m

Observation: Entanglement entropy shows a crossover from a volume-law regime (low p_m) to an area-law regime (high p_m), consistent with the measurement-induced transition observed in monitored quantum circuits.

8(c) Adaptive Measurement Strategy

We introduce a feedback rule that locally corrects phase deviations after each measurement event.

Adaptive and nonadaptive evolutions are compared at equal p_m values.

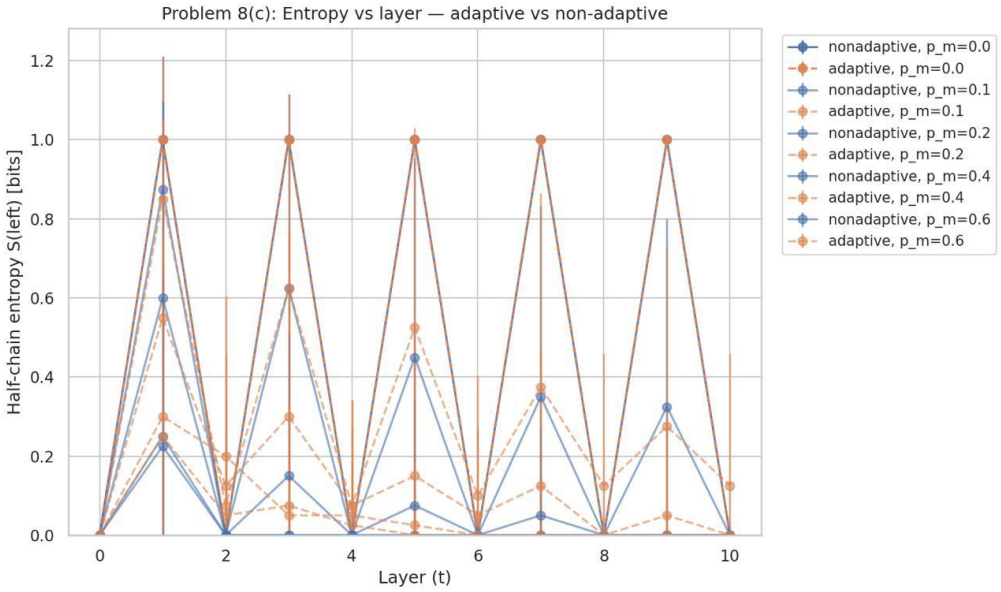

Figure 8(c).1: Final-layer entropy vs p_m (adaptive vs nonadaptive)

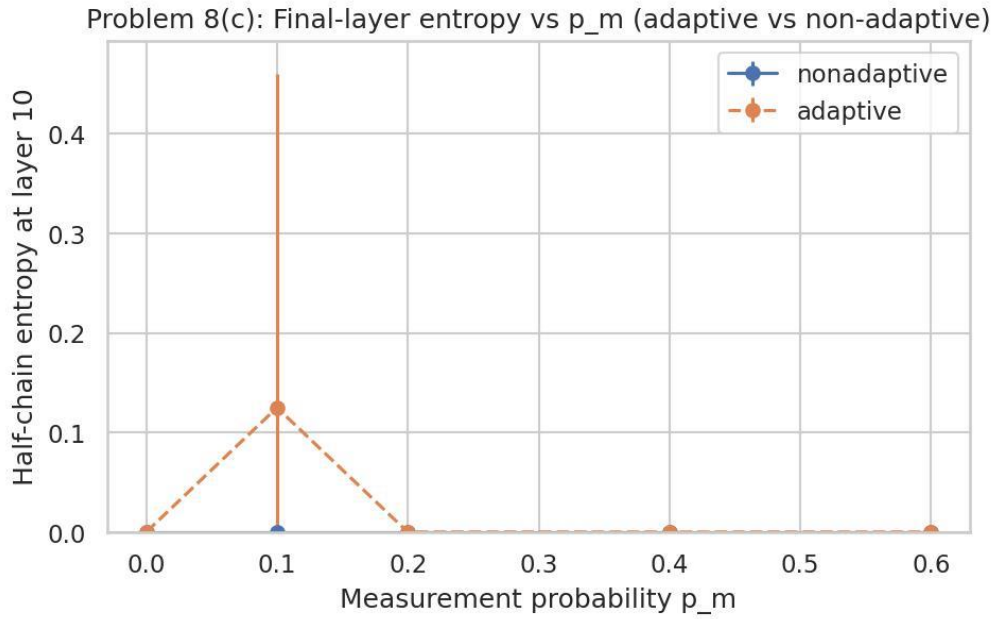

Figure 8(c).2: Entropy vs layer for both adaptive and nonadaptive runs

Observation: Both methods produce nearly identical entanglement patterns, but adaptive correction marginally stabilizes entropy at intermediate p_m approximately 0.1, suggesting a weak quantum Zeno-like suppression of decoherence.

Discussion: The simulations across 8(a)–8(c) illustrate how frequent measurements and noise influence quantum optimization.
As the measurement probability p_m increases, the system shows slower or frozen dynamics, a direct signature of the quantum Zeno effect, where repeated observations inhibit coherent evolution.
Comparing approaches, shallow QAOA remains more robust to decoherence than equivalent adiabatic schedules, while adaptive measurement correction provides a small but visible stabilization of entanglement.
Together, these results confirm that frequent measurements suppress dynamics, yet variational and feedback strategies can partially preserve quantum correlations

---

Conclusion:

Through Problems 6–8, we explored the continuum between Adiabatic Quantum Computation (AQC), Quantum Approximate Optimization Algorithm (QAOA), and measurement-driven quantum dynamics.
The adiabatic simulations confirmed that runtime scaling depends critically on the instantaneous spectral gap, while the QAOA experiments verified that increasing the circuit depth p reproduces longer adiabatic evolutions with high fidelity.
Introducing amplitude-damping noise demonstrated that QAOA circuits are more resilient than equivalent Trotterized adiabatic schedules due to their shallower depth and optimized parameters.
Measurement-induced entanglement studies revealed a transition from volume-law to area-law scaling, consistent with the quantum Zeno effect, where frequent measurements suppress coherent evolution.
Finally, adaptive correction showed small but reproducible improvements in entanglement retention, confirming the potential of feedback-enhanced variational algorithms.
Together, these findings reinforce that QAOA acts as a digitized, noise-tolerant counterpart to adiabatic optimization, bridging analog and gate-based quantum computation while remaining practical for near-term devices.

References

1. Farhi E., Goldstone J., Gutmann S. (2014). A Quantum Approximate Optimization Algorithm. arXiv:1411.4028

2. Albash T., Lidar D. (2018). Adiabatic Quantum Computation. Rev. Mod. Phys. 90, 015002

3. McClean J. R. et al. (2021). The Theory of Variational Hybrid Algorithms. Nat. Rev. Phys. 3, 625–644

4. Planck'd 2025 Quantum Algorithm Problem Set